



# In-Fiber Structured Particles and Filament Arrays from the Perspective of Fluid Instabilities

Bingrui Xu<sup>1</sup> · Shuqi Ma<sup>2,3</sup> · Yuanzhuo Xiang<sup>2,3</sup> · Jing Zhang<sup>4</sup> · Meifang Zhu<sup>5</sup> · Lei Wei<sup>4</sup> · Guangming Tao<sup>2,3</sup> · Daosheng Deng<sup>1</sup>

Received: 12 November 2019 / Accepted: 15 December 2019 / Published online: 7 January 2020  
© The Author(s) 2020

## Abstract

In-fiber structured particles and filament array have been recently emerging, providing unique advantages of feasible fabrication, diverse structures and sophisticated functionalities. This review will focus on the progress of this topic mainly from the perspective of fluid instabilities. By suppressing the capillary instability, the uniform layered structures down to nanometers are attained with the suitable materials selection. On the other hand, by utilizing capillary instability via post-drawing thermal treatment, the unprecedented structured particles can be designed with multimaterials for multifunctional fiber devices. Moreover, an interesting filamentation instability of a stretching viscous sheet has been identified during thermal drawing, resulting in an array of filaments. This review may inspire more future work to produce versatile devices for fiber electronics, either at a single fiber level or in large-scale fabrics and textiles, simply by manipulating and controlling fluid instabilities.

**Keywords** Fiber · Structured particles · Filament arrays · Fluid instabilities · Thermal drawing

## Introduction

The intriguing fluid instabilities are ubiquitous in a host of daily phenomena with beautiful patterns, while being essential for many technological advancements and applications [1–4]. For example, the classical capillary instability appears from faucet dripping to ink-jet printing, during which a cylindrical liquid thread breaking up into a series of droplets to reduce surface energy [3]. The dewetting instability controls or affects adhesion dynamics and surface coating, during which a thin liquid sheet with thickness down to hundreds of nanometers spontaneously ruptures into an array of droplets arising from the van der Waals force [5, 6].

Thermal drawing has been a well-developed technique for producing kilometer-long silica fibers with uniform dimensions in the telecommunication industry, during which a preform is heated at an elevated temperature into a viscous state and stretched into extended fibers by applied tension [7, 8]. Over the last decade, this technique has been successfully employed to achieve an altogether different class of multi-material multi-functional fibers [9]. This specially designed fiber is composed of distinctive components (e.g., semiconductors, insulators, and metals) and complex geometries (e.g., wires, cylindrical shells or layer structures), enabling the sophisticated integrated functionalities (e.g., electronic,

---

✉ Lei Wei  
wei.lei@ntu.edu.sg

✉ Guangming Tao  
tao@hust.edu.cn

✉ Daosheng Deng  
dsdeng@fudan.edu.cn

<sup>1</sup> Department of Aeronautics and Astronautics, Fudan University, Shanghai 200433, China

<sup>2</sup> State Key Laboratory for Modification of Chemical Fibers and Polymer Materials, Donghua University, 2999 North Renmin Road, Songjiang District, Shanghai 201620, China

<sup>3</sup> Wuhan National Laboratory for Optoelectronics, School of Optical and Electronic Information, Huazhong University of Science and Technology, Wuhan 430074, China

<sup>4</sup> School of Electrical and Electronic Engineering, Nanyang Technological University, 50 Nanyang Avenue, Singapore 639798, Singapore

<sup>5</sup> State Key Laboratory for Modification of Chemical Fibers and Polymer Materials, International Joint Laboratory for Advanced Fiber and Low-dimension Materials, College of Materials Science and Engineering, Donghua University, 2999 North Renmin Road, Songjiang District, Shanghai 201620, China

optoelectronic, and acoustic), at either a single-fiber level or in large-scale fabrics and textiles, for a broad range of applications in biomedical, optoelectronic and micro/nano technologies [9–13].

Typically, the process of thermal process is extremely stable that the structure and geometry of cross-section is well preserved from the preform into the fiber with only a simple scaling down in feature size by suppressing capillary instability, leading to periodic dielectric structures for photonic bandgap fiber [9]. (For the well-developed 2D hollow-core photonic crystal fibers, the same capillary instability leads to the surface smoothness of silica glass during fabrication process, resulting in the intrinsic scattering to be responsible for the ultimate optical loss [14].) Nevertheless, recently the capillary instabilities has been successfully utilized into post-drawing process to achieve structured particles and their assemblies for multifunctional devices [11, 12, 15]. Moreover, an intriguing filamentation instability of a stretching viscous sheet during thermal drawing opens new opportunities to achieve unprecedented micro/nanostructures with feasible fabrication, massive production, and versatile functionalities [16–19].

In this review, we will explore in-fiber micro/nano-structures from the perspectives of fluid instabilities. First, the theory of capillary instability is briefly reviewed. Then by suppressing the capillary instability during thermal drawing process, the prescribed structures and geometries of cross section from preform to the fiber can be preserved down to nanometers. On the other hand, by utilizing the capillary instability via post-drawing process, various structured

particles and particle assemblies can be attained. In addition, these structured particles offer more opportunities for diverse fiber devices. Moreover, the observation and mechanism of filamentation instability of a stretching viscous sheet during thermal drawing will be presented. Lastly, the relevant challenges and opportunities of in-fiber structures are discussed.

## Brief Review of Capillary Instability

The study of capillary instability (Fig. 1a) has a long history. In 1849, Plateau identified the intrinsic mechanism associated with the surface tension, since breakup reduces the surface area and the associated surface energy [20]. Lord Rayleigh performed linear stability analysis to quantitatively characterize the growth rate dependent on wavelength, and found that a small disturbance is magnified exponentially with time [21]. (This capillary instability is also referred as Rayleigh-Plateau (RP) instability.) Subsequently, Tomotika investigated the effect of viscosity of the surrounding fluid, which delays or slows down the growth rate [22].

## Reduction of Surface Energy

For a liquid thread which is simplified into a perfect long cylindrical shape, the surface energy is proportional to the surface area for a deformed cylindrical shape. The perturbations can be decomposed into a series of independent modes (Fourier series) with wavelength ( $\lambda$ ) and an amplitude  $\epsilon$ .

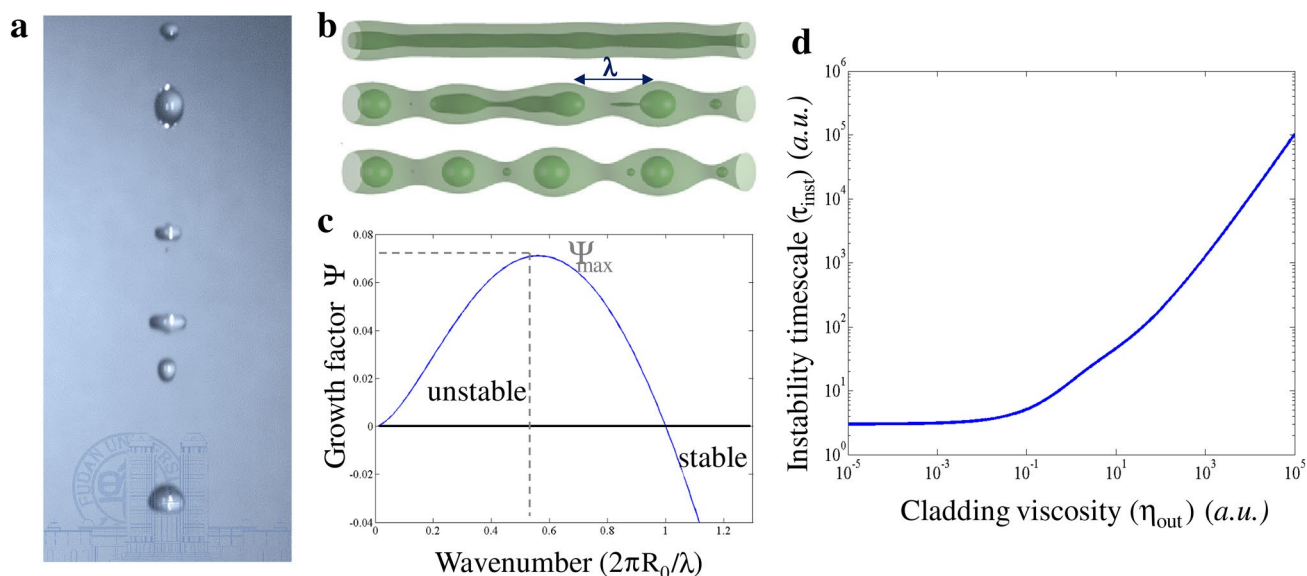


**Fig. 1** Classical capillary instability. **a** High-speed imaging of a liquid jet subjected to capillary instability; **b** Evolution of capillary instability [15]; Reproduced with permission [15]. Copyright 2012,

Springer Nature. **c** Growth factor dependent on wavelength; and **d** Instability timescale ( $\tau_{\text{inst}}$ ) as a function of viscosity of outer or surrounding fluids ( $\eta_{\text{out}}$ ) ( $\eta_{\text{inn}} = 1$ )

Then Under the constrain of volume conservation for an incompressible liquid, the surface energy is expressed as below,

$$E^{\text{surf}}(\lambda) = E_0^{\text{surf}} + \frac{\pi\gamma}{2\lambda R_0} [(2\pi R_0)^2 - \lambda^2]\epsilon^2, \tag{1}$$

where  $E_0^{\text{surf}}$  is the surface energy of a perfect cylindrical thread,  $\gamma$  the interfacial tension, and  $R_0$  is the radius of the liquid thread. For the short wavelength ( $\lambda < 2\pi R_0$ ), the last term of Eq. 1 always becomes positive (regardless of  $\epsilon, \gamma$ ), hence the surface energy will increase and the perturbation is unfavorable. However, for the longer wavelength that satisfies with the following criteria,

$$\lambda > 2\pi R_0, \tag{2}$$

the surface energy always decreases with the amplified perturbation, consequently subjecting to capillary instability to minimize the surface energy (Fig. 1b).

### Growth Rate and Instability Timescale

Further, the linear stability analysis describes the dynamics of perturbation amplitude  $\epsilon(t, \lambda)$  evolving exponentially with time at a certain growth rate  $\omega$ ,

$$\epsilon(t, \lambda) = \epsilon(0)\exp\{i\omega t\}. \tag{3}$$

Qualitatively, this growth rate is related with physical properties of liquid, and can be expressed as below,

$$\omega = \omega(\eta_{\text{inn}}, \eta_{\text{out}}, \gamma, R_0, \lambda) = \frac{\gamma\Psi(\lambda, \eta_{\text{out}}/\eta_{\text{inn}})}{\eta_{\text{out}}R_0}, \tag{4}$$

where  $\eta_{\text{inn}}, \eta_{\text{out}}$  are the viscosity of inner fluid and outer fluid, and  $\Psi$  is the growth factor which is a complicated Bessel functions dependent on wavelength for the given liquids [22]. As shown in Fig. 1c, at the long wavelength

( $\Psi < 0, \omega < 0$ ), the amplitude of perturbation gradually decays with time, resulting in stability. Otherwise, at longer wavelength ( $\Psi > 0, \omega > 0$ ), the amplitude of perturbation gradually increases with time, resulting in instability. At a certain wavelength, the largest  $\Psi_{\text{max}}$  corresponds to the fastest growth of instability  $\omega_{\text{max}}$ .

By varying  $\eta_{\text{inn}}, \eta_{\text{out}}$  typically related with thermal drawing, the timescale of this instability ( $\tau_{\text{inst}}$ ) is determined by this fastest growth rate among various wavelength,

$$\tau_{\text{inst}} \sim \omega_{\text{fast}}^{-1} \sim \max_{\lambda} [\Psi(\lambda, \eta_{\text{out}}/\eta_{\text{inn}})/\eta_{\text{out}}]^{-1}. \tag{5}$$

As shown in Fig. 1d, for the given  $\eta_{\text{inn}}=1$ , the higher  $\eta_{\text{out}}$  results in longer  $\tau_{\text{inst}}$  to delay or suppress instability.

Besides a cylindrical core, the capillary instability of a cylindrical shell with equal viscosities [23] or concentric cylindrical shells [24] has been studied theoretically as well. These theoretical results can provide helpful guidance to either suppress or enhance instability through selecting suitable materials or controlling fabrication process for the community in materials science and optical fibers.

### Suppressing Capillary Instability for Uniform Layered Structures During Thermal Drawing

By suppressing capillary instability, uniform layer thicknesses have been demonstrated in flexible polymer fibers (Fig. 2a). SEM micrographs (Fig. 2b–d) clearly reveals the high-quality multiple-layer structures with thicknesses down to micrometers and tens of nanometers [9, 18].

### Radial-Stability Criterion

The process of thermal drawing is extremely complicated, involving many physical parameters and their coupling (e.

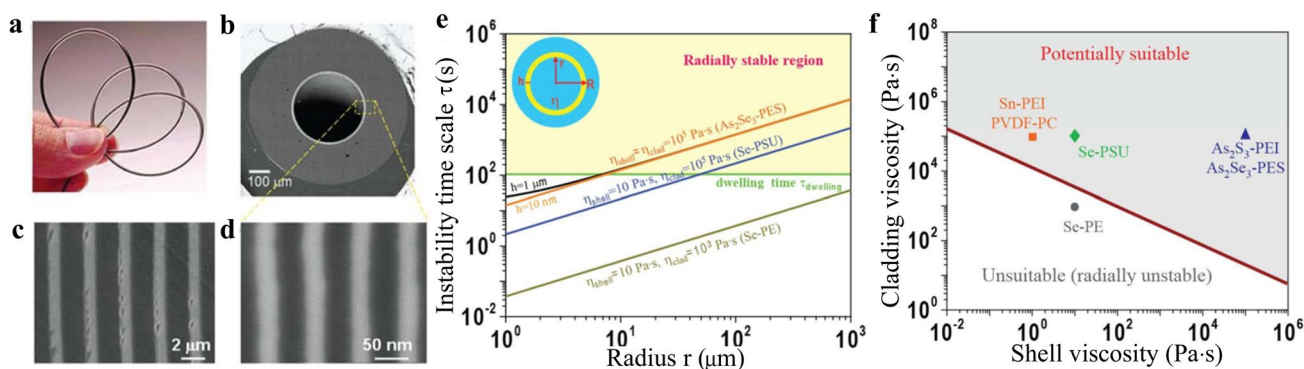


**Fig. 2** In-fiber cylindrical shells with thickness down to micro/nanometers by suppressing capillary instability. **a** Photograph of fiber. **b** SEM of fiber cross-section; Magnified view of multilayer structures reveals the thickness of micrometer (c) and tens of nanometers (d),

respectively. **e**, Radial stability map, and inset for cross-sectional geometry of cylindrical shell in calculation. **f** Material selection map for various shell-cladding viscous combination [18]

g., heating transfer, flow field, and temperature-dependent viscosity, and necking effect). As a first step toward understanding, only a single fluid instability, i.e., capillary instability resulting in radial fluctuations for a cylindrical fluids, is investigated. Consequently, the stability criteria offers the necessary (although not sufficient) condition to maintain the uniform layered structures [18], proving the theoretical guidance for the materials selection and structure design, and particularly to exclude certain materials combinations for fiber drawing as well.

The instability time scale ( $\tau_{\text{inst}}$ ) is calculated over a broad range of physical parameters including geometry [e.g. radius ( $R$ ) and shell thickness ( $h$ )] and materials properties (viscosity) (Fig. 2e). The dwelling time ( $\tau_{\text{dwelling}}$ ) is defined by the time of materials in viscous state before exiting hot furnace to be frozen in fiber during thermal drawing (typically  $\tau_{\text{dwelling}} \approx 100$  s). By comparing these two timescales, the radial stability criterion ( $\tau_{\text{inst}} > \tau_{\text{dwelling}}$ ) implies that the instability is delayed or suppressed. On the other hand, the radius fluctuations alone will render the shell unstable ( $\tau_{\text{inst}} < \tau_{\text{dwelling}}$ ), resulting in the fast development and growth of instability. For example, the time scale for  $\eta_{\text{shell}} = 10$  Pa · s,  $\eta_{\text{clad}} = 10^5$  Pa · s, corresponding to Se–PSU, indicates the stability of shells of radius  $R \approx 250$   $\mu\text{m}$ , consistent with the experimental observation.

## Materials Selection Map

Given the viscosities and surface tension of a particular material pair, we can use Fig. 2e to determine whether that pair is suitable for drawing: if it is radially unstable, then it is almost certainly unsuitable, whereas if it is radially stable then the pair is at least potentially suitable. Each materials combination can be classified by whether it falls in the radially stable ( $\tau > \tau_{\text{dwelling}}$ , yellow region) or radially unstable ( $\tau < \tau_{\text{dwelling}}$ , white region), as shown in Fig. 2e.

These materials combinations are presented in Fig. 2f [18]. The boundary line ( $\tau = \tau_{\text{dwelling}}$ ) divides the map into two areas. The shaded area above the boundary line is the region of potentially suitable materials combinations for fiber drawing ( $\text{As}_2\text{Se}_3$ –PES,  $\text{As}_2\text{S}_3$ –PEI, Se–PSU); while the materials combinations below the boundary line are unsuitable due to radial instability (Se–PE). Moreover, since a high viscosity cladding improves stability, a wider variety of shell materials with low viscosity may possibly be employed, such as the metals Sn and In. These various available classes of metals, polymers and semiconductors expand the potential functionalities of devices in microstructured fibers.

## Utilizing Capillary Instability for Structured Particles Via Post-Drawing Thermal Process

Instead of suppressing capillary instability, interestingly one can deliberately utilize the instability to generate a variety of micro/nanostructures with novel functionalities by employing the post-drawing thermal treatment, such as inducing in-fiber capillary instability. Actually, this post-drawing process is a general approach for all the fibers in a broad sense, which are produced by many different approaches besides thermal drawing [9–12, 25], including electrospinning [26–28], melt spinning [29], solution spinning, gel spinning [30] (Fig. 3a). The capillary instability of these continuous fibers via thermal treatment results in the discrete particles and their assemblies in a high throughput, chemically clean manner (Fig. 3b).

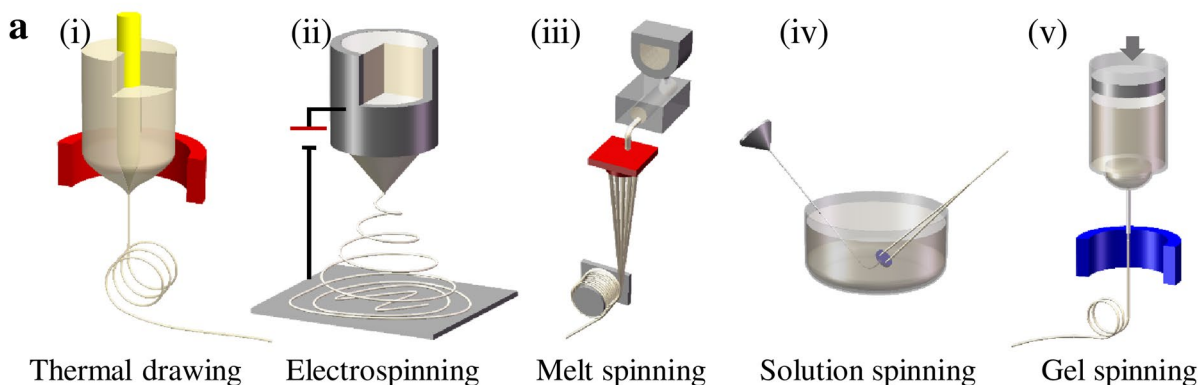
## Digital Design of Particle Structures

By heating a solid cylindrical-shaped core embedded into a fiber at an elevated temperature, capillary instability generates scalable fabrication of uniformly sized spherical particles, with the size ranges from millimeters down to tens of nanometers [15]. Interestingly, the structured particles with various internal structure (e.g., Janus, core-shell, or beach ball) was demonstrated by heating the structured core to trigger instability [15]. Moreover, the digital design of structured photonic particle was studied by accurately distributing the high refractive-index contrast materials independently within its 3D architecture (Fig. 3c) [31].

By tuning various physical parameters such as viscosity and surface tension through different thermal modulation at spatial, time, material domains, both the particle material and morphology library have been expanded in several ways. Biomaterial like bio-functional coating or biocompatible packaged biological core was integrated into particles [32]. Development of spatial selective [25] or material selective [33] thermal profile for optoelectronic material pair with high viscosity contrast leads to the fabrication of Si spheres and bispherical Si ‘p–n molecule’ devices. Even further complexity in digital preform design was highlighted for solely or combined radial and azimuthal control on particles [31]. In addition, control on solidification front and recrystallization, microstructure and stress control on SiGe alloy spheres was demonstrated for bandgap modification and in-fiber microelectronics [34].

Non-spherical structures were also fabricated based on controlled plastic deformation during breakup process [35], templates [36, 37], inverse capillary instability under solvothermal reaction [38], and solvent vapor

### Fiber Fabrication



### Fiber to Particles & Particle Assemblies

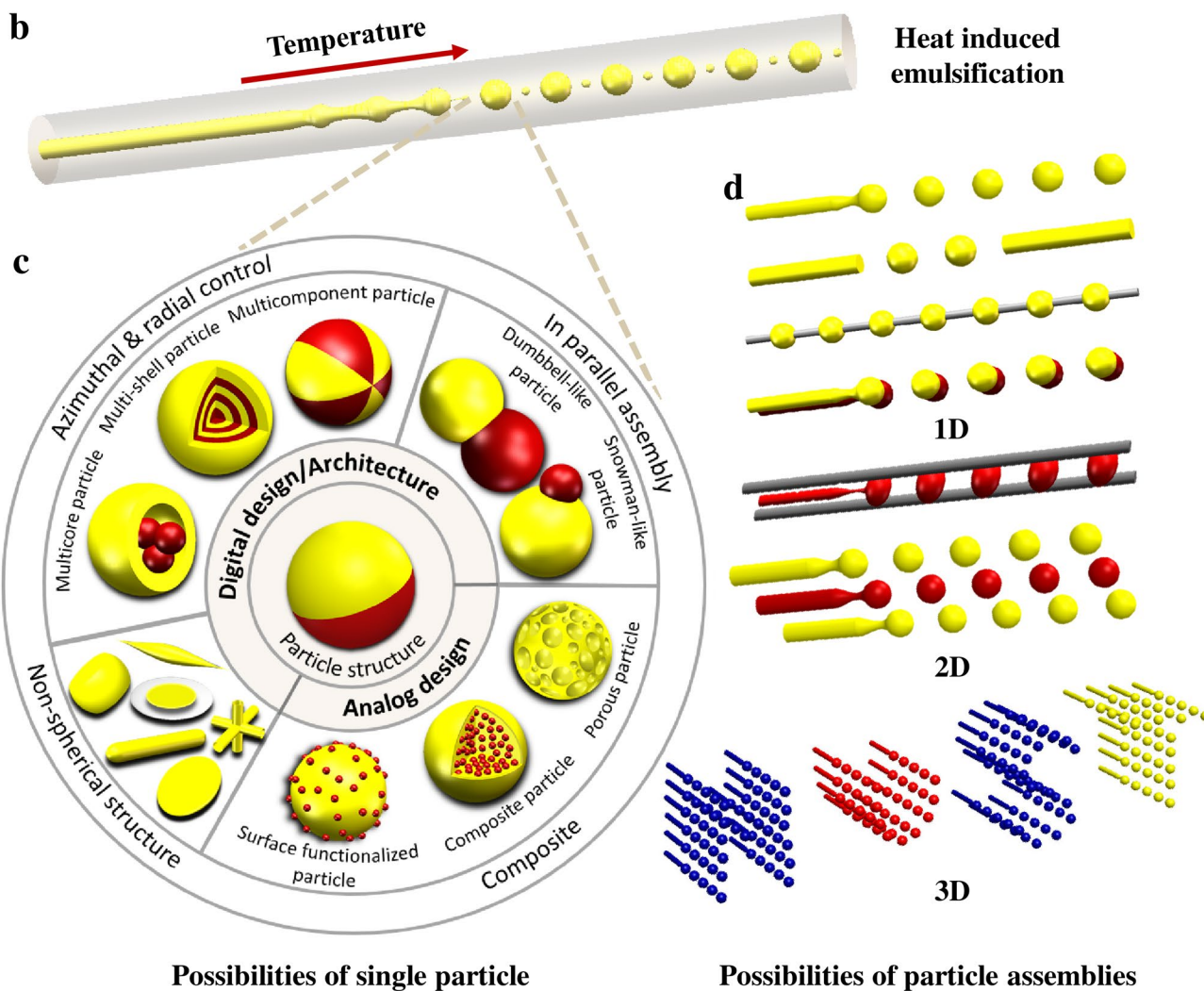


**Fig. 3** The structure design of particles and particle arrays via in-fiber capillary instability. **a** Illustration of several fiber fabrication methods. (i) Thermal drawing method. (ii) Electrospinning. (iii) Melt spinning. (iv) Solution spinning. (v) Gel spinning. **b** In-fiber morphology evolution under a temperature gradient map. **c** Division and examples

of in-particle digital and analog design to a wide range of materials (e.g., glasses, thermoplastic polymers, metals, semiconductor, composite). **d** Illustration of well-ordered one-, two- and three-dimensional arrays of functional particles

annealing [39]. Moreover, an extra design dimension for desired functionality by adding composite into our material library, such as the fabrication of porous spheres [40], quantum dots composite particles and magnetic-polymeric composite particles [41]. Indeed, much progress of integrating multiple materials into a single particle to achieve multiple functionalities has been made.

### Digital Design of Particle Assemblies

These structured particles remain frozen in situ as a new form of metamaterials or devices and are identified as inner suspended discrete micro/nanostructure (Fig. 3d). For example, with the ultra-smooth surface resulted from fluid instability, spherical, or sphere-based chalcogenide-glass particles [35] or Si spheres [33] with tapered optical fiber can be assembled to build high Q-factor microresonator. Besides, selectively heating can transform the middle semiconducting core of a tri-core fiber into a train of spherical particles, which bridges the side carbon polyethylene composite [42] or metal [43] electrodes, therefore constructing long but discrete photodetecting devices. This general in-fiber fluid instability was also explored to fabricate metal nanoparticles [44] and well-dispersed metal-polymer nanocomposite [45]. More future works should be required to extend many possibilities of functional devices based on this special fabrication method (Fig. 3d).

### Structured-Particle-Based Multifunctional Fiber Devices and their Applications

Deep investigation and precise control of the in-fiber capillary instability induced by thermal treatments have been paving a new way to generate a variety of micro/nanostructures with novel functionalities. In this section, we briefly review the particle-based multifunctional fiber devices and their remarkable contributions in biomedical, optoelectronic and micro/nano technologies.

#### Polymeric Micro- and Nanoparticles for Biosensing and Encapsulation

Currently, synthesizing functional polymeric micro- and nanoparticles are of great significance in biomedicine and therapeutics as biosensors, biomarkers and drug-delivery carriers [32]. However, conventional methods for producing these particles are limited in the little polymer species, the monotonous morphology and the small size range. The thermal treatment induced in-fiber capillary instability offers methods to overcome these traditional limitations. The developed process can generate uniformly sized spherical polymer particles with continuously tunable diameters from

the millimeter scale down to 50 nm. A typical example of the fabrication process is illustrated in Fig. 4a: a polymer fiber with target core/cladding materials and designed structure is achieved by the fiber thermal drawing process and capillary instability is induced by the heating furnace to generate the functional spherical particles. The particles can be easily designed by only changing the structure of the fiber preform and be biocompatible by using biomaterials, ideal for volume encapsulation and surface functionalization. For example, microcapsules of biological materials in collagen-filled polymer-shell are achieved by this approach, which can be useful for cosmetics and biomedicine applications. The collagen was injected into a 50  $\mu\text{m}$  diameter hollow core fiber in which acyclic olefin polymer layer line the polysulfone cladding, then the capillary instability was induced to generate collagen-filled polymeric microcapsules. While coating the polymeric particles with antibodies or antigens would make these spheres useful in biodetection and immunoassay [32].

#### Multi-material Structured Particles Fiber Device

The ability to generate diversities of in-sphere structures is of significant interest. As shown in Fig. 4b, core-shell spheres, Janus spheres, beach ball spheres and multilayer spheres were achieved by the fibers with structured cores [15]. As the fiber preform is constructed at the macroscale, complex fiber geometries can be achieved by judiciously structuring over the core in the radial direction (core-shell and multilayer spheres) and azimuthal structure (Janus and beach ball spheres) [31]. The structured fiber core is surrounded by a polymer matrix and it transforms into multi-material particles during the thermal treatment. This approach to generate structured multi-material particles has several important features. First, uniformly sized spherical particles with a wide range of diameters from 20 nm to 2 mm can be fabricated. Second, it can produce large numbers of structured particles by the breakup phenomenon of high-density parallelizing cores in the same fiber. Such particles demonstrate a superior performance serving as polarization-dependent optical scattering elements with a tailoring scattering efficiency. Furthermore, with doping materials, the in-fiber generated structured spheres gain more functionalities such as emitting fluorescence, expanding their capabilities in photonics and bio-imaging.

#### Metal-Polymer Nanocomposite Fibers

Thermally induced capillary stability promises a scalable generation of polymer fibers with metal micro/nano composites, which have unique physicochemical advantages for electronics, energy and biological applications. The polymer fiber patterned with neatly arranged and well dispersed metal nanoparticles that can present better tuned electromagnetic

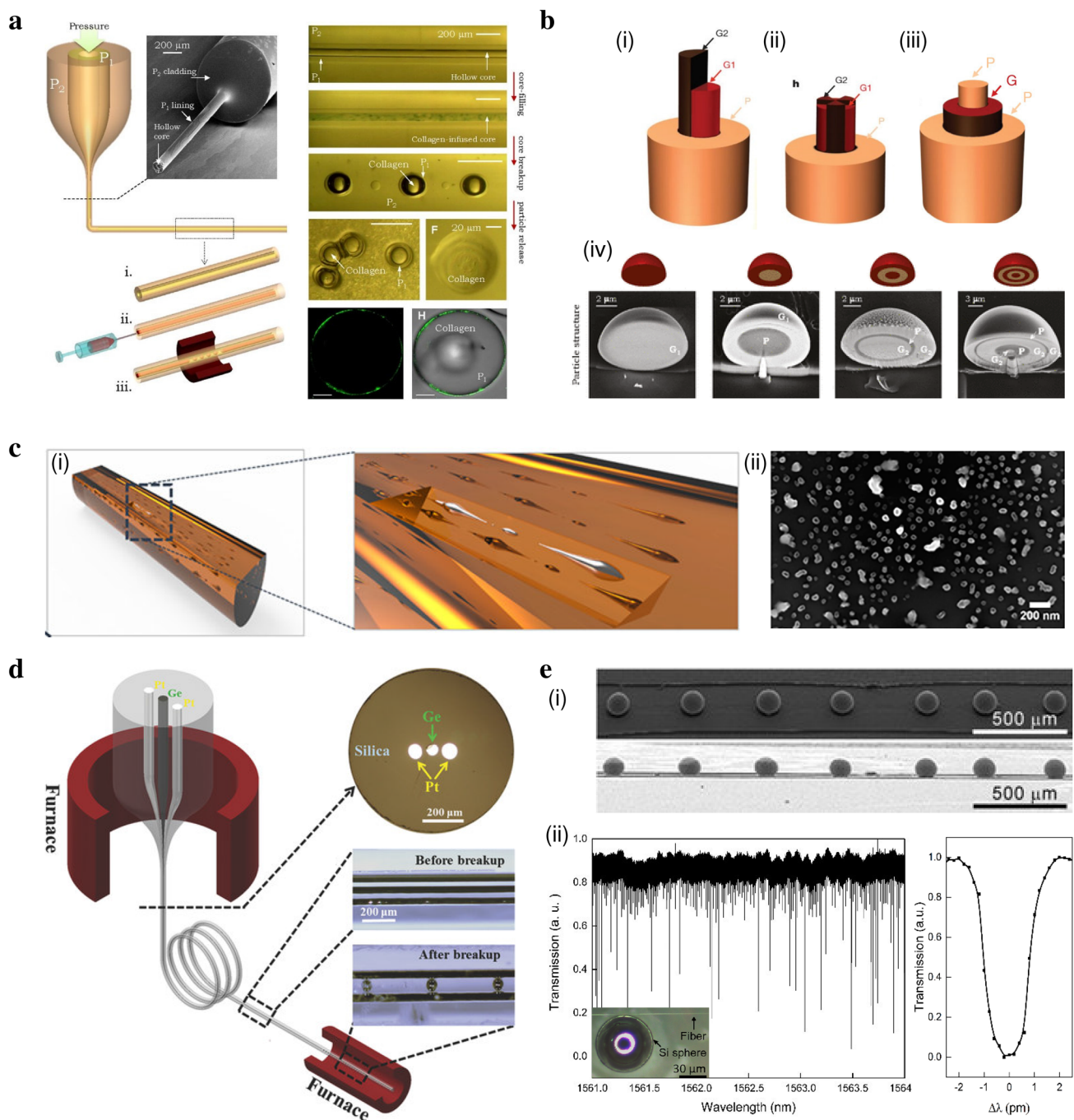


**Fig. 4** Applications of particle-based multifunctional fiber devices. **a** Fabrication of collagen-filled microcapsules.  $P_1$ : cyclic olefin polymer;  $P_2$ : polysulfone. Reproduced with permission [32]. Copyright 2013, National Academy of Sciences. **b** Fabrications of multi-material structured spherical particles [15, 31]. (i) Schematic diagram of the fiber preform for the Janus particles. (ii) Schematic diagram of the fiber preform for the beach ball particles. (iii) Schematic diagram of the fiber preform for the core-shell structured particles. (iv) Schematic diagrams and SEM micrographs of the core-shell and multilayer particles cross-sections.  $G_1$ :  $As_2S_3$ ;  $G_2$ :  $Ge_{1.3}(As_2Se_3)_{98.7}$ ;  $P$ : polyethersulfone. Reproduced with permission [15]. Copyright 2012, Springer Nature. Reproduced with permission [31]. Copyright 2016, National Academy of Sciences. **c** PES polymer fiber with Sn metal

nanoparticles. (i) Schematic of metal-polymer nanocomposite fiber. (ii) SEM image of Sn nanoparticles [45]. Reproduced with permission [45]. Copyright 2016, ASME. **d** Fabrication of optoelectronic fibers based on break-to-contact approach [43]. Reproduced with permission [43]. Copyright 2017, WileyVCH. **e** High-Q microcavity resonator arrays. (i) Top and profile SEM micrographs of  $As_2Se_3$  WGM resonator arrays. The average size of the spherical particles is 124.4  $\mu m$  [35]. (ii) Transmission spectra of a silicon spherical particles of 60  $\mu m$  in diameter. The quality factor  $Q$  of the WGM resonator mode is  $7.1 \times 10^5$ . Inset shows the coupling of evanescent light into the spherical particle resonator by a tapered silica fiber [33]. Reproduced with permission [35]. Copyright 2014, WileyVCH. Reproduced with permission [33]. Copyright 2017, WileyVCH

properties and higher strength properties [45]. To achieve this type of fiber, a fabrication of PES (polyethersulfone) fibers with parallelizing Sn cores is demonstrated as an example, which are produced by a multi-stage iterative size reduction thermal drawing process. The earlier thermal drawing processes reduce the size of the polymer fiber and produce a remarkably long fiber with dozens of Sn cores, then in the later processes, the thermal induced in-fiber capillary instability transfers these fiber cores into a large number of nanoparticles (Fig. 4c). This method promises a nanomanufacturing process to polymer fiber with well-aligned metal particles in high throughput, leading to a variety of new functionalities.

### Optoelectronic Fibers and Photodetecting Devices

Optoelectronic fibers and photodetecting devices are being developed based on the selective amplification of in-fiber capillary instability. Based on a precisely defined electrode-semiconductor-electrode triaxial core fiber, a fully functional optoelectronic in-silica device is achieved by employing Plateau-Rayleigh instability in fiber (Fig. 4d). As mentioned in the last section, the heating process will transfer the functional materials into a viscous liquid state and lead the continuous core to breakup into a chain of spheres. Differing from transferring all cores into spheres, the selective amplification only breaks semiconductor core into a chain of spheres taking the advantage of distinct melting points between the semiconductor materials and the electrode materials as well as accurate temperature control. For electrical connection in the fiber, the semiconductor spheres with larger diameters than the core would create contacts onto the continuous electrode cores directly, forming a fully functional in-fiber optoelectronic device. On the basis of the above principles,  $\text{As}_2\text{Se}_3$  core/carbon polyethylene composite electrodes [42] and germanium core/platinum electrodes optoelectronic fibers [43] have been achieved. The break-to-contact technology can create  $\sim 10^4$  self-assembled and entirely packaged spherical photodetecting devices per meter of the fiber.

### High-Q Microcavity Resonator Arrays

The ability of fabricating uniform-sized particles with ultra-smooth surface and crystalline structure create an opportunity to achieve high-Q whispering gallery mode (WGM) resonator arrays. WGM resonators with high-quality factor (Q) and small mode volumes are widely investigated in biosensing, micro-lasing, optical signal processing, and nonlinear optics. The micro- and nano-spherical particle generation based on in-fiber capillary instability open a new route for fabricating the high-quality three-dimensional microcavity resonator arrays [35] (Fig. 4e). The spherical particles

fabricated from this method feature an ultra-smooth surface roughness owing to the high surface tension and large built-in stress during their formation, which is an extraordinary platform for developing optical resonators. In general, target functional materials ( $\text{As}_2\text{Se}_3$  and silicon) are firstly made into the rods and drawn into a fiber with suitable cladding materials by the thermal drawing process. Followed by the thermal treatment processing, the continuous fiber cores eventually break into chains of spheres due to the in-fiber Plateau-Rayleigh instability. These spheres ultra-smooth surface, perfectly spherical shape and uniform diameters are confirmed with AFM and SEM, which performed  $3.1 \times 10^5$  high-Q factor with  $\text{As}_2\text{Se}_3$  particles [33] and  $7.1 \times 10^5$  high-Q factor with Si particles [35] as WGM micro-resonator arrays. It is worth noting that, this fabrication method can be seamlessly applied to other semiconductors (Ge and  $\text{Bi}_2\text{Te}_3$ ) and silica.

### Identifying Filamentation Instability of a Stretching Viscous Sheet

In-fiber micro/nanostructures, such as uniform layered structures or structured particles, can be manipulated by either suppressing the well-known capillary instability during thermal drawing or utilizing it via post-drawing process. Furthermore, as the feature size of geometries is reduced down to micro/nano-scale during thermal drawing, new physical phenomena might possibly occur.

### Observation of Filamentation Instability

An instability phenomenon has been identified during a thermal drawing where a viscous sheet, subjected to a unidirectional stretching, evolves into an array of continuous filaments arranged orderly [16, 17] rather than droplets (for example, in spinodal dewetting of a thin sheet or in capillary-instability breakup of a cylindrical jet), as shown in Fig. 5a. In this phenomenon, stability is preserved along the longitudinal (stretching) direction, while instability occurs exclusively along the transverse (perpendicular to the stretching) direction. Therefore, the term ‘anisotropic instability of a stretching viscous sheet’ (AISVS) is used for this physical phenomenon.

### Physical Mechanism

Since AISVS phenomenon was observed at the microscopic length scale, van der Waals forces should play an important role, similar to dewetting phenomena. Moreover, the effect of stretching for a sheet is analogous to that of a continuous falling viscous jet under gravity, and hence



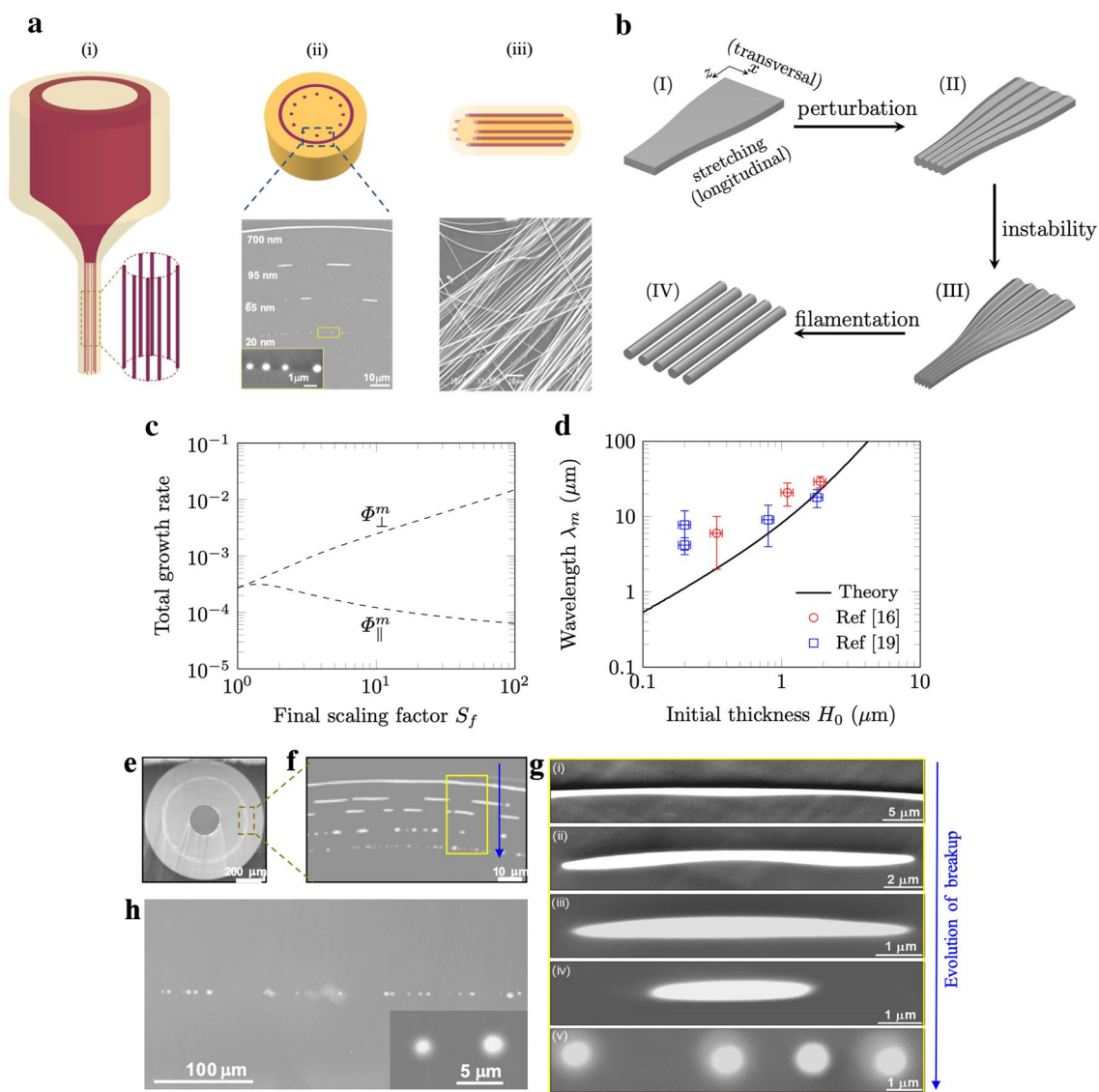


**Fig. 5** The identified filamentation instability. **a** Filamentation instability during a process of thermal drawing (i) sketch; (ii) transversal instability at the reduced thickness; (iii) Longitudinal stability [16]. Reprinted (adapted) with permission from [16]. Copyright (2008) American Chemical Society. **b** Sketch for the mechanism of anisotropic instability of a stretching viscous sheet; **c** Anisotropic instabil-

ity arising from stretching, maximum total growth rates  $\Phi_{\perp}^m$  and  $\Phi_{\parallel}^m$ ; **d** For PSU/Se/PSU, the predicted wavelength agrees with the measured experimental wavelength; **e–h** SEM imaging for the evolution of the transversal instability and the experimental wavelength. **b–h** Reprinted figures with permission from [19]. Copyright (2019) by the American Physical Society

the longitudinal instability is suppressed [46]. Thus, the physical mechanism for AISVS is proposed by combining stretching and van der Waals forces in Fig. 5b: (I) a viscous sheet undergoes elongation deformation; (II) perturbations are amplified in the transverse direction; (III) the longitudinal stability is suppressed compared to the transverse stability; (IV) consequently, this anisotropic instability results in an array of filaments. (Here the curvature is neglected since the radius are much larger than the thickness.)

**Linear Theory**

In the model, a viscous thin sheet with thickness  $H_0$ , velocity  $w_0$ , and width  $2\ell_0$  at the inlet, sandwiched within another fluid, is stretched by a drawing force over a length  $L$  to the take-up speed  $w_f$ . For a stretching thin sheet, the attenuation rates of thickness and width are  $S_H = H_0/H$  and  $S_{\ell} = \ell_0/\ell$  respectively. And then along the longitudinal direction, stretching extends the length of fluid elements at a rate  $S_{\perp}S_{\parallel}$  due to the flow continuity. Hence, the velocity ( $w$ ), the wave number of a perturbation along the stretching direction ( $k_{\parallel}$ ),

that along the transverse direction ( $k_{\perp}$ ), and the sheet thickness ( $H$ ) are related by

$$\begin{aligned} w/(S_H S_{\ell}) &= w_0, & k_{\parallel} S_H S_{\ell} &= \text{const}, \\ k_{\perp}/S_{\ell} &= \text{const}, & H S_H &= \text{const}. \end{aligned} \quad (6)$$

Stretching changes the perturbation growth (i.e., the instability development) along the two directions. To quantitatively evaluate this effect, a total growth rate is obtained by integrating local growth rate  $\omega(k, H)$  [19, 46]. This dispersion relation of a viscous uniform sheet sandwiched by another viscous fluid was studied [19, 24].

Consequently, the total growth rate along the longitudinal stretching direction ( $\Phi_{\parallel}$ ) and transverse direction ( $\Phi_{\perp}$ ) for perturbations introduced at position  $z_p$  are

$$\begin{aligned} \Phi_{\parallel}(z_p, k_{\parallel}) &= \int_{t_p}^t \omega_{\parallel}[k_{\parallel}(\tau), H(\tau)] d\tau \\ &= \int_{z_p}^L \frac{1}{w_0 S_{\ell}(\xi) S_H(\xi)} \\ &\quad \times \omega_{\parallel} \left[ k_{\parallel}(z_p) \frac{S_H(z_p) S_{\ell}(z_p)}{S_H(\xi) S_{\ell}(\xi)}, H(z_p) \frac{S_H(z_p)}{S_H(\xi)} \right] d\xi, \end{aligned} \quad (7a)$$

$$\begin{aligned} \Phi_{\perp}(z_p, k_{\perp}) &= \int_{t_p}^t \omega_{\perp}[k_{\perp}(\tau), H(\tau)] d\tau \\ &= \int_{z_p}^L \frac{1}{w_0 S_{\ell}(\xi) S_H(\xi)} \\ &\quad \times \omega_{\perp} \left[ k_{\perp}(z_p) \frac{S_{\ell}(\xi)}{S_{\ell}(z_p)}, H(z_p) \frac{S_H(z_p)}{S_H(\xi)} \right] d\xi. \end{aligned} \quad (7b)$$

Here the time integral has been transformed into a spatial integral by using the local-velocity relationship  $d\tau = d\xi/w = d\xi/(w_0 S_{\ell} S_H)$ . The instability should be dominated by the fastest total growth rate along both directions respectively, i.e.,  $\Phi_{\parallel}^m = \max[\Phi_{\parallel}(z_p, k_{\parallel})]$ ,  $\Phi_{\perp}^m = \max[\Phi_{\perp}(z_p, k_{\perp})]$ .

Considering a perturbation is introduced at the starting point  $z_p = 0$  at one-dimensional ‘fiber limit’ with  $S_H = S_{\ell}$  [refs], the fastest total growth rate along the longitudinal directions ( $\Phi_{\parallel}^m$ ) and the transversal direction ( $\Phi_{\perp}^m$ ) as a function of the final scaling factor  $S_f$  (attenuation rate at  $z = L$ ,  $S_f = S_H(L) = S_{\ell}(L)$ ) are presented in Fig. 5c. The longitudinal instability can be suppressed by the stretching effect ( $S_f > 1$ ) whereas the transverse instability is dramatically enhanced. Therefore, an anisotropic instability phenomenon appears ( $\Phi_{\parallel}^m < \Phi_{\perp}^m$ ) and becomes more striking at larger  $S_f$ .

### Theory Consistent with Observation

These theoretical predictions are further compared with experimental results for AISVS. For PSU/Se/PSU, growth

rate  $\Phi_{\perp}^m$  is calculated for different initial thickness  $H_0$  and perturbations introduced at any point  $z_p \in (0, L)$ . The theoretical breakup wavelength is obtained from  $\lambda_m = 2\pi S(z_m)/(k_{\perp}^m S_f)$ , where perturbations with wavenumber  $k_{\perp}^m$  introduced at  $z_m$  have the fastest growth rate  $\Phi_{\perp}^m$ .

During thermal drawing, the produced structures are frozen or solidified into the fiber, allowing both cross-sectional and axial inspection with spatial resolution down to nanometers through SEM. Consequently, the quantitative conclusions for stability limits of the feature size can be made, allowing the visualization of evolution of transversal instability (Fig. 5e–h). The experimental wavelength ( $\lambda_{exp}$ ) is measured as the average space of Se filament arrays in SEM images of fiber cross sections. The experimental results [16, 19] agree well with the theory in Fig. 5d.

### Outlook

Here we mainly focus on the perspective of fluid instabilities to overview in-fiber nanostructures. The effect of stress or viscoelasticity of non-Newtonian fluid during thermal drawing is beyond the scope, and actually during polymer cold-drawing, the stress can cause controllable and sequential fragmentation of the core to produce nanorods [47].

This fabrication method of structured particles via post-drawing thermal treatment highly depends on a physical mechanism of fluid instabilities and the subsequent breakup, as opposed to the chemical synthesis. This method has been paving a new way for broad applications including but not limited to electronic devices, photovoltaics, medicine and healthcare, targeted drug delivery, biology, chemical sensing, and cosmetics. Such a process can achieve spherical particles from a variety of materials with disparate optical, electronic, magnetic and thermal properties with a wide range of processing temperature from 400 to 2400 K and 10 orders of difference in fiber core/cladding viscosity ratio regardless of the crystal structures [9, 12].

An unavoidable limitation in the isothermal method is the precise control on the resulting sphere sizes, as the isothermal break-up process constantly lead to the formation of satellite spheres, which is still a complex route to be controllable. As an ideal heating source in the thermal treatment due to its narrow operating wavelength, small beam size, highly stable output and tunable power, CO<sub>2</sub> laser has been demonstrated to precisely control the molten core/cladding interface, which leads to the formation of spherical particles with uniform diameters in a full spectrum of diameters from micro- to nano-scale [48].

Although remarkable development has been made in the field of functional structured particles, by using a single particle and particle assemblies as a platform, the optimization of material selection and the fully designable distribution

of micro/nanofillers in matrix may lead to intriguing new physical phenomena and practical applications. Further improvements can be realized by the optimization of fiber fabrication process such as controlling the drawing stress to achieve a more uniform fiber core, which will lead to a smaller variation of the resulting sphere sizes. Moreover, the ability to induce a precisely tunable built-in stress onto spherical particles and to form in-fiber homo- and hetero-junctions may offer a substantial impact on future developments of photonic, electric, thermoelectric devices, and other related fields [11–13].

Moreover, the filamentation instability of a stretching sheet during thermal drawing clearly offers more opportunities to explore fluid instability, and unconventional sophisticated nanostructures might be achieved through designing structures such as filamentation in two adjacent sheets or three-layer sandwiched sheets. By utilizing the available toolbox of various materials combination (such as semiconductors, metals, and polymers) compatible with thermal drawing, more versatile functional nanodevices are anticipated to be realized in either single fibers or mass-produced in large-scale textiles [11–13, 49].

**Acknowledgements** Guangming Tao acknowledges the National Natural Science Foundation of China (Grant No. 61875064), WNLO Man-Machine Lab Fund, WNLO Innovation Fund and HUST Innovation Fund (Grant No. 2172018KFYXKJC021), and State Key Laboratory for Modification of Chemical Fibers and Polymer Materials, Donghua University. Lei Wei acknowledges the support by the Singapore Ministry of Education Academic Research Fund Tier 2 (MOE2015-T2-2-010), Singapore Ministry of Education Academic Research Fund Tier 1 (MOE2019-T1-001-103 and MOE2019-T1-001-111), and the EEE Ignition Research Grant. Daosheng Deng is indebted to Prof. Yoel Fink, Prof. Steven Johnson, and Prof. Howard Stone for the guidance and discussions on the topic of in-fiber nanostructures generated by fluid instabilities, and the collaboration with Prof. Ayman Abouraddy; acknowledges the funding support by the National Young Thousand Talent Program in China and startup from Fudan University.

**Open Access** This article is licensed under a Creative Commons Attribution 4.0 International License, which permits use, sharing, adaptation, distribution and reproduction in any medium or format, as long as you give appropriate credit to the original author(s) and the source, provide a link to the Creative Commons licence, and indicate if changes were made. The images or other third party material in this article are included in the article's Creative Commons licence, unless indicated otherwise in a credit line to the material. If material is not included in the article's Creative Commons licence and your intended use is not permitted by statutory regulation or exceeds the permitted use, you will need to obtain permission directly from the copyright holder. To view a copy of this licence, visit <http://creativecommons.org/licenses/by/4.0/>.

## References

- Oron A, Davis SH, Bankoff SG. Long-scale evolution of thin liquid films. *Rev Mod Phys.* **1997**;69:931–80.
- Craster RV, Matar OK. Dynamics and stability of thin liquid films. *Rev Mod Phys.* **2009**;81(3):1131–98.
- Eggers J. Nonlinear dynamics and breakup of free-surface flows. *Rev Mod Phys.* **1997**;69(3):865–930.
- de Gennes PG, Brochard-Wyart F, Quere D. Capillarity and wetting phenomena. Berlin: Springer; 2004.
- Reiter G. Dewetting of thin polymer films. *Phys Rev Lett.* **1992**;68(1):75–8.
- Reiter G. Unstable thin polymer films: rupture and dewetting processes. *Langmuir.* **1993**;9(5):1344–51.
- Keck DB, Maurer RD, Schultz PC. On the ultimate lower limit of attenuation in glass optical waveguides. *Appl Phys Lett.* **1973**;22(7):307–9.
- Agrawal GP. Fiber optic communication systems. New York: Wiley; 2010.
- Abouraddy AF, Bayindir M, Benoit GJ, Hart SD, Kuriki K, Orf ND, Shapira O, Sorin F, Temelkuran B, Fink Y. Towards multimaterial multifunctional fibres that see, hear, sense and communicate. *Nat Mater.* **2007**;6(5):336–47.
- Tao G, Stolyarov AM, Abouraddy AF. Multimaterial fibers. *Int J Appl Glass Sci.* **2012**;3(4):349–68.
- Yan W, Page AG, Nguyendang T, Qu Y, Sordo F, Wei L, Sorin F. Advanced multimaterial electronic and optoelectronic fibers and textiles. *Adv Mater.* **2019**;31(1):1802348.
- Loke G, Yan W, Khudiyev T, Noel G, Fink Y. Recent progress and perspectives of thermally drawn multimaterial fiber electronics. *Adv Mater.* **2019**. <https://doi.org/10.1002/adma.201904911>.
- Yan W, Dong C, Xiang Y, Jiang S, Leber A, Loke G, Xu W, Hou C, Zhou S, Cheng M, Hu R, Shum P, Wei L, Jia X, Sorin F, Tao X, Tao G. Thermally drawn advanced functional fibers: new frontier of flexible electronics. *Mater Today.* **2020**. <https://doi.org/10.1016/j.mattod.2019.11.006>.
- Roberts PJ, Couny F, Sabert H, Mangan BJ, Williams DP, Farr L, Mason M, Tomlinson A, Birks TA, Knight JC, et al. Ultimate low loss of hollow-core photonic crystal fibres. *Opt Express.* **2005**;13(1):236–44.
- Kaufman JJ, Tao G, Shabahang S, Banaei E, Deng D, Liang X, Johnson SG, Fink Y, Abouraddy AF. Structured spheres generated by an in-fibre fluid instability. *Nature.* **2012**;487(7408):463–7.
- Deng D, Orf ND, Abouraddy AF, Stolyarov AM, Joannopoulos JD, Stone HA, Fink Y. In-fiber semiconductor filament arrays. *Nano Lett.* **2008**;8(12):4265–9.
- Deng D, Orf ND, Danto S, Abouraddy AF, Joannopoulos JD, Fink Y. Processing and properties of centimeter-long, in-fiber, crystalline-selenium filaments. *Appl Phys Lett.* **2010**;96(2):023102.
- Deng D, Nave J, Liang X, Johnson SG, Fink Y. Exploration of in-fiber nanostructures from capillary instability. *Opt Express.* **2011**;19(17):16273–90.
- Xu B, Li M, Wang F, Johnson SG, Fink Y, Deng D. Filament formation via the instability of a stretching viscous sheet: physical mechanism, linear theory, and fiber applications. *Phys Rev Fluids.* **2019**;4:073902.
- Plateau J. Statique experimentale et theorique des liquides soumis aux seules forces moleculaires. Paris: Gauthier-Villars; 1873.
- Rayleigh L. On the instability of jets. *Proc Lond Math Soc.* **1878**;1:4–13.
- Tomotika S. On the instability of a cylindrical thread of a viscous liquid surrounded by another viscous fluid. *Proc R Soc Lond A.* **1935**;150(870):322–37.
- Stone HA, Brenner MP. Note on the capillary thread instability for fluids of equal viscosities. *J Fluid Mech.* **1996**;318:373–4.
- Liang X, Deng D, Nave J, Johnson SG. Linear stability analysis of capillary instabilities for concentric cylindrical shells. *J Fluid Mech.* **2011**;683:235–62.

25. Gumennik A, Wei L, Lestoquoy G, Stolyarov AM, Jia X, Reke-meyer PH, Smith MJ, Liang X, Grena BJ, Johnson SG, et al. Silicon-in-silica spheres via axial thermal gradient in-fiber capillary instabilities. *Nat Commun*. **2013**;4(1):2216.
26. Wu J, Wang N, Zhao Y, Jiang L. Electrospinning of multilevel structured functional micro-/nanofibers and their applications. *J Mater Chem*. **2013**;1(25):7290–305.
27. Xue J, Wu T, Dai Y, Xia Y. Electrospinning and electrospun nanofibers: methods, materials, and applications. *Chem Rev*. **2019**;119(8):5298–415.
28. Huang W, Xiao Y, Shi X. Construction of electrospun organic/inorganic hybrid nanofibers for drug delivery and tissue engineering applications. *Adv Fiber Mater*. **2019**;1(1):32–45.
29. Naeimirad M, Zadhoush A, Kotek R, Neisiany RE, Khorasani SN, Ramakrishna S. Recent advances in core/shell bicomponent fibers and nanofibers: a review. *J Appl Polym Sci*. **2018**;135(21):46265.
30. Cui Y, Gong H, Wang Y, Li D, Bai H. A thermally insulating textile inspired by polar bear hair. *Adv Mater*. **2018**;30(14):1706807.
31. Tao G, Kaufman JJ, Shabahang S, Naraghi RR, Sukhov S, Joannopoulos JD, Fink Y, Dogariu A, Abouraddy AF. Digital design of multimaterial photonic particles. *Proc Natl Acad Sci USA*. **2016**;113(25):6839–44.
32. Kaufman JJ, Ottman R, Tao G, Shabahang S, Banaei E, Liang X, Johnson SG, Fink Y, Chakrabarti R, Abouraddy AF. In-fiber production of polymeric particles for biosensing and encapsulation. *Proc Natl Acad Sci USA*. **2013**;110(39):15549–54.
33. Zhang J, Li K, Zhang T, Buenconsejo PJS, Chen M, Wang Z, Zhang M, Wang Z, Wei L. Laser induced in-fiber fluid dynamical instabilities for precise and scalable fabrication of spherical particles. *Adv Funct Mater*. **2017**;27(43):1703245.
34. Gumennik A, Levy E, Grena BJ, Hou C, Rein M, Abouraddy AF, Joannopoulos JD, Fink Y. Confined in-fiber solidification and structural control of silicon and silicongermanium microparticles. *Proc Natl Am*. **2017**;114(28):7240–5.
35. Aktas O, Ozgur E, Tobail O, Kanik M, Huseyinoglu E, Bayindir M. A new route for fabricating onchip chalcogenide microcavity resonator arrays. *Adv Opt Mater*. **2014**;2(7):618–25.
36. Deng X, Paven M, Papadopoulos P, Ye M, Wu S, Schuster T, Klapper M, Vollmer D, Butt H. Solvent-free synthesis of micro-particles on superamphiphobic surfaces. *Angewandte Chemie*. **2013**;52(43):11286–9.
37. Gupta TD, Martinmonier L, Yan W, Bris AL, Nguyendang T, Page AG, Ho K, Yesilkoy F, Altug H, Qu Y, Sorin F. Self-assembly of nanostructured glass metasurfaces via templated fluid instabilities. *Nat Nanotechnol*. **2019**;14(4):320–7.
38. Ma L, Peng J, Wu C, He L, Ni Y. Sphere-to-tube transition toward nanotube formation: a universal route by inverse plateaurayleigh instability. *ACS Nano*. **2017**;11(3):2928–33.
39. Chiu Y, Liu C, Weng C, Chiu T, Li J, Chen J. Sunny-side-up egg-shaped structures: surface modification to form anisotropic polymer particles driven by the plateau Rayleigh instability as fluorescence manipulation platforms. *Macromolecules*. **2019**;52(4):1601–8.
40. Grena BJ, Alayrac J, Levy E, Stolyarov AM, Joannopoulos JD, Fink Y. Thermally-drawn fibers with spatially-selective porous domains. *Nat Commun*. **2017**;8(1):364.
41. Du M, Ye S, Tang J, Lv S, Chen J, Orava J, Tao G, Lan P, Hao J, Yang Z, et al. Scalable in-fiber manufacture of functional composite particles. *ACS Nano*. **2018**;12(11):11130–8.
42. Rein M, Levy E, Gumennik A, Abouraddy AF, Joannopoulos JD, Fink Y. Self-assembled fibre optoelectronics with discrete translational symmetry. *Nat Commun*. **2016**;7(1):12807.
43. Wei L, Hou C, Levy E, Lestoquoy G, Gumennik A, Abouraddy AF, Joannopoulos JD, Fink Y. Optoelectronic fibers via selective amplification of in-fiber capillary instabilities. *Adv Mater*. **2017**;29(1):1603033.
44. Zhao J, Javadi A, Lin T, Hwang I, Yang Y, Guan Z, Li X. Scalable manufacturing of metal nanoparticles by thermal fiber drawing. *J Micro Nano Manuf*. **2016**;4(4):041002.
45. Lin T, Zhao J, Cao C, Javadi A, Yang Y, Hwang I, Li X. Fabrication of metalpolymer nanocomposites by in-fiber instability. *J Micro Nano Manuf*. **2016**;4(4):041008.
46. Javadi A, Eggers J, Bonn D, Habibi M, Ribe NM. Delayed capillary breakup of falling viscous jets. *Phys Rev Lett*. **2013**;110(14):144501.
47. Shabahang S, Tao G, Kaufman JJ, Qiao Y, Wei L, Bouchenot T, Gordon AP, Fink Y, Bai Y, Hoy RS, et al. Controlled fragmentation of multimaterial fibres and films via polymer cold-drawing. *Nature*. **2016**;534(7608):529–33.
48. Zhang J, Wang Z, Wang Z, Zhang T, Wei L. In-fibre particle manipulation and device assembly via laser induced thermocapillary convection. *Nat Commun*. **2019**;10(1):5206.
49. Zhu M, Kikutani T, Liu T, Ramakrishna S, Tao G. Fiber changes our life. *Adv Fiber Mater*. **2019**;1(1):1–2.